Title	Intensification of surface enhanced Raman scattering of thiol-containing molecules using Ag@Au core@shell nanoparticles
Author(s)	Singh, Prerna; Thuy, Nguyen, T. B.; Aoki, Yoshiya; Mott, Derrick; Maenosono, Shinya
Citation	Journal of Applied Physics, 109(9): 094301-1-094301-7
Issue Date	2011-05-02
Type	Journal Article
Text version	publisher
URL	http://hdl.handle.net/10119/9830
Rights	Copyright 2011 American Institute of Physics. This article may be downloaded for personal use only. Any other use requires prior permission of the author and the American Institute of Physics. The following article appeared in Prerna Singh, Nguyen T. B. Thuy, Yoshiya Aoki, Derrick Mott, and Shinya Maenosono, Journal of Applied Physics, 109(9), 094301 (2011) and may be found at http://link.aip.org/link/doi/10.1063/1.3579445
Description	

Intensification of surface enhanced Raman scattering of thiol-containing molecules using Ag@Au core@shell nanoparticles

Prerna Singh,[1,2] Nguyen T. B. Thuy,[1] Yoshiya Aoki,[1] Derrick Mott,[1] and Shinya Maenosono[1,a)]
[1]*School of Materials Science, Japan Advanced Institute of Science and Technology, 1-1 Asahidai, Nomi, Ishikawa 923-1292, Japan*
[2]*Department of Chemistry, University of Delhi, Delhi, 110007, India*

(Received 11 February 2011; accepted 21 March 2011; published online 2 May 2011)

In this paper, we study the relationship between nanoparticles' structure/composition and the chemical nature of the molecules to be identified in surface enhanced Raman scattering (SERS) spectroscopy. Three types of nanoparticles (NPs) were synthesized, including Ag, Au, and silver coated by gold (Ag@Au), in order to study the resulting enhancement effects. When a rhodamine 6G dye molecule was used to assemble the NPs, it was found that Ag NPs exhibited the highest enhancement activity. However, when a thiol containing 3-amino-1,2,4-triazole-5-thiol molecule was used to assemble the NPs, it was found that the Ag@Au NPs exhibited high Raman activity as well as the Ag NPs. The results give insight into how the chemical properties of the molecules to be analyzed play an important role in the SERS detection. An additional parameter of the analysis reveals the relative stability of the three types of NP probes synthesized with regard to oxidation in the presence of different mediating molecules and varying salt concentrations. The results are of interest in designing and employing NP probes to detect biological molecules using colorimetric and SERS based approaches. © *2011 American Institute of Physics*. [doi:10.1063/1.3579445]

I. INTRODUCTION

Nanoparticles (NPs) have received much attention due to their potential applications in various fields, for example, catalysis, thermoelectric materials, drug delivery, microelectronics, sensing, and many other emerging areas of nanotechnology.[1–4] Specifically, metal NPs have garnered interest as biologically sensitive probes to detect molecules such as DNA, RNA, proteins, amino acids, etc. Silver and gold are well known in this field. The optical properties of silver NPs make it an exceptional candidate for use in biodiagnostics and sensing.[2,5,6] Gold is highly desirable as a nanoscale probe because of its resistance to oxidation and beneficial reactivity with the sulfur component of many biomolecules.[5,6] In order to take advantage of the beneficial properties of both silver and gold in a single functional nanoparticle probe, many researchers have tried to couple silver and gold as a single core@shell structure (Ag@Au) with enhanced optical properties from the Ag core and resistance to oxidation/sulfur reactivity from the Au shell.[7] The optical properties of these metal NPs can be tuned by changing the size of the Ag core and the thickness of the Au shell, etc., leading to tailorable Ag@Au NP bioprobes.

An important aspect in harnessing the novel properties of this class of NPs for biomolecular sensing and recognition is the manipulation and control of the interparticle properties, i.e., NP surface properties, interparticle distance, assembly, etc. There are several studies that focus on exploiting the interfacial properties of nanostructures such as place-exchange reactions of ligands,[8] layer-by-layer stepwise assembly,[9] DNA linked assembly,[10] polymer or dendrimer mediated molecular recognition,[11,12] hydrogen-bonding mediated assembly,[13] and multidentate thioether mediated assembly.[14] For applications in chemical sensing (see Zheng *et al.* in Ref. 13; Refs. 15–17), nanoelectronics (see Musick *et al.* in Ref. 9; Ref. 18), and medical diagnostics,[10,19] the molecularly mediated assemblies of NPs are often used as a detection route. As one increasingly important class of nanostructures, the immobilization of dye molecules onto NPs has captured recent interest with regard to exploiting its optical properties for chemical and biological applications, including the fluorescence quenching of small dye molecules on NPs,[20,21] complementary oligonucleotides for single stranded DNA linked metal NPs or bar-coded metal nanowires,[22–24] and fluorescent-dye-doped NPs for medical diagnostics and labeling.[25] Although extinction, absorption, and scattering are still the primary optical properties of interest, other spectroscopic techniques are also beginning to take advantage of the novel properties of metal NPs.

Recently, various metal NP based biosensors using localized surface plasmon resonance (LSPR) have been proposed.[26–30] One of the most attractive extensions of LSPR sensors is their biosensing application using surface enhanced Raman scattering (SERS).[31–37] SERS is a surface sensitive phenomenon that results in the enhancement of Raman scattering by molecules adsorbed on rough metal surfaces. The significant amplification of Raman scattering intensity occurs because of the electric field enhancement present in the vicinity of small, interacting metal NPs that are illuminated with light resonance at or near the LSPR frequency. SERS is of great importance because of its ability to detect extremely low concentrations of analytes, even at the single-molecule level, for biological diagnostics.[38] SERS has

[a)]Author to whom correspondence should be addressed. Electronic mail: shinya@jaist.ac.jp.

been employed in nanodiagnostics to detect biological molecules such as proteins, DNA, etc. with high selectivity and sensitivity by using Raman labels conjugated to NPs, as SERS based biosensors are highly sensitive.[39–42] However, despite this excitement and interest, there have been few studies that identify which type of metallic NP probe is optimal for use in a given application, as the interaction of the molecule to be detected with the Raman probe is one of the keys to the observed enhancement.

Therefore, we propose an easy approach to study the fundamental interactions between the NP based SERS probes and the molecules to be detected. The analysis relies on the assembly of the NPs using two kinds of molecular linker systems with vastly different chemical properties, and then quantifying and comparing the resulting Raman enhancement observed for the different particle–molecule combinations. The study is designed to address the question of whether Ag@Au NPs (which are expected to show the highest Raman enhancement) are superior to Ag or Au monometallic NP probes. For the first linker system, rhodamine 6G dye (R6G) is used to assemble the NPs, relying on electrostatic interactions in the adsorption of the molecule to the NP surface. The second linker system used is a thiol containing molecule, 3-amino-1,2,4-triazole-5-thiol (ATT), which adsorbs to the NP surface via the sulfur functionality. Both molecules lead to the spontaneous assembly of the different nanoparticle systems. The resulting assemblies exhibit Raman enhancement, which is quantified to determine the effectiveness of the individual NP probes. We then compare the Raman enhancement for the three different NPs, i.e., Ag, Au, and Ag@Au. The results show that the chemical nature of the molecule used in the assembly plays an important role in the exhibited enhancement. As an additional parameter, the relative stability of the different NP probes was found to vary significantly in varying salt concentrations, which also has implications with regard to using these probes in practical biomolecular detection systems.

II. EXPERIMENTAL DETAILS

A. Chemicals

Silver nitrate ($AgNO_3$) 99.9999%, sodium acrylate 97%, trisodium citrate (SC) 99.0%, sodium chloride (NaCl) 99.0%, gold tetrachloroaurate trihydrate ($HAuCl_4{\cdot}3H_2O$) 99.9%, and common solvents were obtained from Aldrich. R6G (practical grade) was obtained from Wako Chemical. We obtained 3-amino-1,2,4-triazole-5-thiol (ATT) 98.0% from Tokyo Chemical Industry. Water was purified with a Millipore Direct-Q system (18.2 MΩ). Dialysis membranes with molecular weight pore size of 10,000 Da were obtained from Spectra/Por and were rinsed in pure water before use.

B. Instrumentation and measurements

Techniques including transmission electron microscopy (TEM), high-resolution TEM (HR-TEM), Raman spectroscopy, energy dispersive x-ray spectroscopy (EDS), and UV-visible spectroscopy (UV-Vis) were used to characterize the size, shape, composition, and other properties of the NPs. TEM analysis was performed on a Hitachi H-7100 instrument operated at 100 kV. HR-TEM was performed on an Hitachi H-9000NAR operated at 300 kV. Raman spectra were obtained with an Ar^+ ion laser (wavelength 514.5 nm, power 50 mW), using a Horiba-Jobin Yvon Ramanor T64000 triple monochromator equipped with a CCD detector. The nonpolarized Raman scattering measurements were set under a microscope sample holder using a 180° backscattering geometry at room temperature. The laser spot diameter was 1 μm. An acquisition time of 60 s per spectrum was used with averaging of three spectra per analysis area. EDS mapping was performed on a JEOL JEM-ARM200F scanning TEM (STEM) operated at 200 kV. Samples for TEM, HR-TEM, and EDS mapping were prepared by dropping the suspended NPs onto a carbon coated copper grid and drying overnight in air. UV-Vis spectra were collected in the range of 300 to 1100 nm using a Perkin-Elmer Lambda 35 UV-Vis spectrometer.

C. Ag NP synthesis

Ag NPs were synthesized via the citrate reduction method.[43] We prepared 50 ml of a 1 mM solution of $AgNO_3$ in a 100 ml round flask. This solution was then purged with argon and stirred with heating until reflux was achieved. Next, 1 ml of a 3.4×10^{-3} mM aqueous solution of SC was added to the refluxing $AgNO_3$ solution. The solution was refluxed for 1 h. After about 3 min of boiling, the solution turned yellow, and after about 5 min it turned gray-yellow and became opaque. The reaction solution was cooled to room temperature after 1 h of refluxing, and then the opaque dispersion was centrifuged at 4000 rpm for 30 min. After the centrifugation, the upper part of the solution became a transparent yellow color. The upper part of the solution was removed and contained the final Ag NPs.

D. Au NP synthesis

For the synthesis of the Au NPs, the general procedure followed was the same as that for the synthesis of the Ag NPs. An aqueous solution of $HAuCl_4{\cdot}3H_2O$ (50 ml, 0.25 mM) was vigorously stirred and heated to reflux at 100 °C. Then, an aqueous solution of SC (0.5 ml, 3.4×10^{-5} mM) was added to the reaction solution. Refluxing was continued for 1 h. The light yellow Au solution turned immediately clear; after 5 min the color changed to purple, and then slowly to dark purple, and over time the solution became a wine red color. After the refluxing, the mixture was cooled to room temperature and used for experiments without further processing.

E. Ag@Au NP synthesis

The as-synthesized citrate-capped Ag NPs were used as core particles in the synthesis of the Ag@Au NPs.[7] The Ag NP dispersion (50 ml) was brought to reflux with stirring, and then $HAuCl_4{\cdot}3H_2O$ (8.31×10^{-7} moles, 10 ml, 0.0831 mM) and SC (8.49×10^{-4} moles, 10 ml, 0.8466 mM) were simultaneously added dropwise. The reaction solution was refluxed for 1 h. The yellow colored solution turned slightly

orange after the coating of Au onto the Ag core. After refluxing, the mixture was cooled to room temperature and used for further experiments.

F. Creation of Raman active NP assemblies

For the three sets of as-synthesized NPs, including Ag, Au, and Ag@Au NPs, the relative concentration of all three samples was made uniform by diluting the concentrated dispersions. The final NP concentration used to create the assemblies was 7.0×10^{-11} M. In a cuvette, 3 ml of the NP dispersion was taken for creating the assemblies using R6G or ATT. In the case of assembly using R6G, NaCl was added to partially screen the negative charge on the NP surfaces. First, 50 μl of 0.1 mM R6G was added. Then, 100 μl of 0.1 M NaCl was added to the NP dispersion, and after 5 min a UV-Vis spectrum was collected to monitor the start of particle assembly. The reaction was monitored for 1 h by taking UV-Vis spectra every 15 min in the range of 300–1100 nm. After 1 h, the UV-Vis spectrum reached a pseudosteady state. In the case of ATT, 10 μl of 1 mM ATT aqueous solution was added to 3 ml of NP dispersion in a cuvette. An immediate change in color was observed—from red to purple for the Au NPs and from yellow to green for the Ag NPs—which indicates a fast interaction of ATT with these NPs. In the case of Ag@Au NPs, the color gradually changed from orange to green. UV-Vis spectra were collected every 15 min for a total of 1.5 h. After 1 h, the UV-Vis spectrum reached a pseudosteady state.

III. RESULTS AND DISCUSSION

A. Assessment of the core@shell structure

The Ag NPs are coated with a layer of Au to form Ag@Au NPs by following a general seeded growth mechanism. Briefly, first the Ag NPs are brought to reflux, and then dilute aqueous Au and SC solutions are added simultaneously so that gold can reduce on the Ag NP surface, causing a layer of Au to form over the Ag cores. The challenges faced in this reaction include the galvanic replacement between Ag and Au, which is partially suppressed by adding additional reducing agent in the coating procedure.[7] Figure 1 shows the normalized UV-Vis absorption spectra of the as-synthesized Ag, Au, and Ag@Au NPs. The LSPR peak wavelengths occur at 403, 525, and 423 nm for Ag, Au, and Ag@Au NPs, respectively. Both the Ag and Au NPs display SPR bands at characteristic frequencies. For the Ag@Au NPs, a single nonsymmetrical peak is observed between those for Ag and Au (only slightly shifted from the orginal Ag peak position), indicating the coating of Au onto the Ag NPs. Figure 2 shows the TEM images of the Ag, Au, and Ag@Au NPs. The TEM images show that all NPs have roughly spherical morphologies (a minor fraction of nanorods forms in the Ag NP synthesis, but the occurrence is too low to significantly impact the optical properties). In addition, slightly darker rings outside the lighter spherical centers are observed in the case of Ag@Au NPs [Fig. 2(c)], indicating the formation of a Au shell on the Ag NP surfaces.[7] The

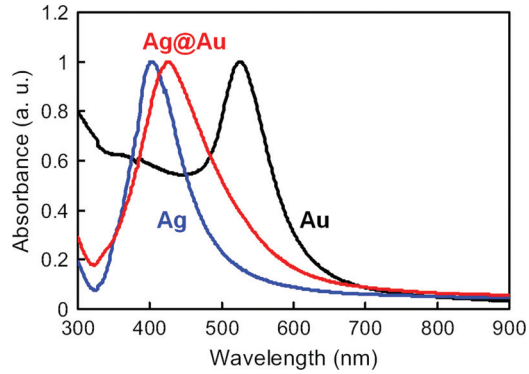

FIG. 1. (Color online) Normalized UV-Vis spectra for as-synthesized Ag, Au, and Ag@Au NPs.

mean size and size distributions are 39.4 ± 6.5 nm for Ag, 43.1 ± 4.3 nm for Au, and 43.9 ± 7.9 nm for Ag@Au NPs.

EDS mapping analysis was conducted to study the relative positions of Ag and Au within the individual Ag@Au NPs. Figure 3 shows the high angle annular dark field (HAADF) image and the elemental mapping images for Ag and Au, as well as an overlay of both. In general, the dark field image reveals NPs with a dense outer shell and a relatively less dense inner area. When comparing this image to the Au map, it is shown that a majority of the gold exists at the periphery of the NPs, which is expected for the formation of a Au shell. However, the Ag map also shows several particles with relatively less Ag in some particle centers. This can be attributed to partial etching of the silver cores as Au is added in the coating procedure. While some etching may take place, a majority of the Ag remains, with a coating of Au forming over it, as can be observed in the overlay map of Ag and Au showing many particles with a majority of Ag concentrated inside the NPs and a majority of the Au concentrated at the periphery (shell) of the NPs.

B. Assembly of NPs using Raman active molecules

The as-synthesized NPs are capped with citrate ions, and so the surfaces of the NPs are negatively charged. Therefore, two types of positively charged Raman active molecules (R6G and ATT; structures shown in Fig. 4) were used to assemble the different NPs. Moreover, the ATT molecule exists in thiol or thione tautomeric forms, and thus a metal–thiol interaction is expected to play a key role in the assembly of the NPs. By assembling NPs, hot spots can be created between adjacent NPs. At the same time, R6G and ATT can act as Raman reporters as well as assembling agents.

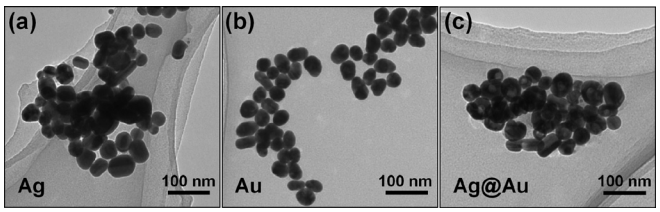

FIG. 2. TEM images of as-synthesized (a) Ag, (b) Au, and (c) Ag@Au NPs.

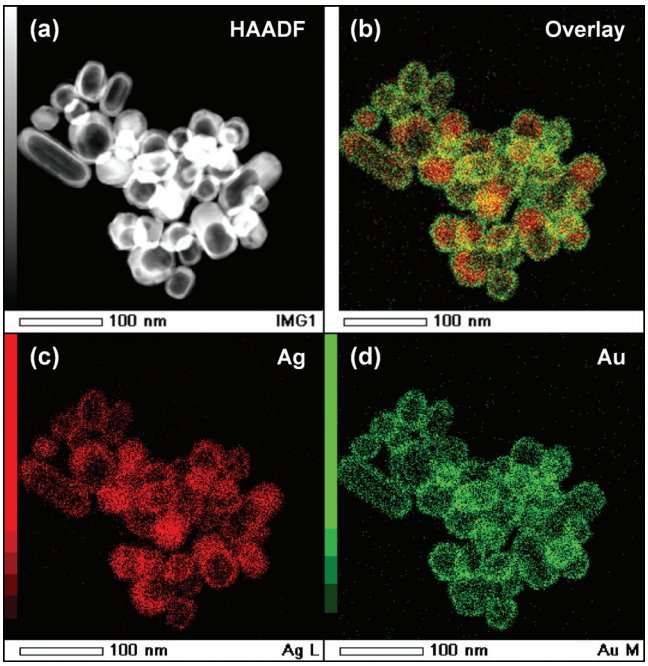

FIG. 3. (Color online) (a) HAADF-STEM image and EDS elemental mapping images of Ag@Au NPs. (b) Overlay of (c) the Ag L edge and (d) the Au M edge illustrates the core-shell structure of the Ag@Au NPs.

Because R6G carries a positive charge and ATT has an amine group that is protonated and also carries a positive charge, the NPs are expected to assemble by the following two mechanisms. For the assembly using R6G, the negative charge on the surface of the NPs electrostatically interacts with the positive charge on the R6G molecules, allowing R6G to adsorb to the NP surface. As the R6G molecules adsorb to the NPs, the negative charge begins to be screened, decreasing the electrostatic repulsive forces between NPs, allowing adjacent NPs to move closer together and begin to assemble. Simultaneously, π–π stacking occurs between dye molecules on adjacent NPs, creating the NP linkage.[44] As this process continues, the NP assembly is formed. In this interaction, the screening effect of only R6G is not enough to cause a kinetically fast assembly of NPs. For this reason, NaCl is added to increase the assembly rate. For the ATT linker molecule, which has a thiol moiety, the assembly mechanism can be explained as follows. The sulfur functionality will adsorb directly to the NP metal surface, forming a metal–sulfur bond (an interaction that is strong for the Au surface and relatively weaker for the Ag surface). Next, the positively charged ATT molecule will interact electrostatically with the negative surface charge (induced by the citrate capping layer) of an adjacent NP, forming a link. As more and more NPs are linked, the assembly is formed. The electrostatic attraction between the amine groups of ATT and citrate ions on the NP surfaces seems to be kinetically fast. Therefore, the assembling process might depend strongly on the metal–sulfur interaction strength. As discussed above, the path of assembly in the cases of R6G and ATT are very different from each other. Hereafter we refer to these assembling processes as *van der Waals driven assembly* (vdWA) and *thiol-mediated Coulomb driven assembly* (TMCA) for the cases of R6G and ATT, respectively. One interesting parameter of the experiment is that the thiol component of the ATT molecule is expected to bind to the Au surface (i.e., Au and Ag@Au NPs) more strongly than to the Ag surface (i.e., Ag NPs). In this case, it would be logical to think that the Au containing NPs would have more ATT molecules adsorbing to the surface, leading to heightened enhancement of the Raman signal. Studying this question is part of the objective of this work.

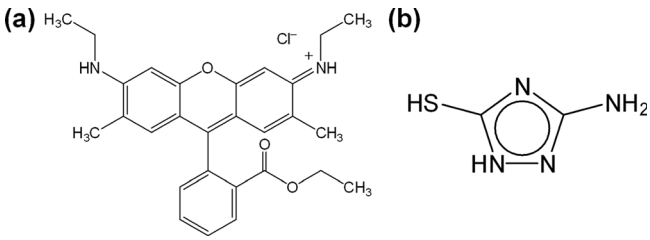

FIG. 4. Chemical structures of (a) R6G and (b) ATT.

The assembly of the NPs is confirmed by the UV-Vis spectra, as shown in Figs. 5 and 6. Figure 5 shows the UV-Vis spectra of NP dispersions before and after adding R6G. After adding R6G molecules to the NP dispersion, a significant reduction in the LSPR intensity and an evolution of an extended SPR (ESPR) band at longer wavelengths can be clearly seen for all NPs. R6G has an absorption peak at around 520 nm, and thus the UV-Vis spectra after adding R6G also contain the contribution of R6G absorption. The emergence of an ESPR band is a definitive sign of the assembly of NPs. Figure 6 shows the UV-Vis spectra of NP dispersions before and after adding ATT. After adding ATT molecules to the NP dispersion, a significant reduction in the LSPR intensity and the appearance of an ESPR band at longer wavelengths can be clearly seen for all NPs. ATT has no absorption peak in the range of 300–900 nm, as shown in Fig. 6.

C. Assessment of the Raman activity

The assemblies were rinsed with pure water and then were dropped onto a (3-aminopropyl)trimethoxysilane-coated glass substrate. The deposited NP assemblies were allowed to dry in air overnight, and then Raman measurements were conducted. Figures 7(a) and 7(b) show the Raman spectra of the vdWA and the TMCA, respectively. In the case of vdWA, the primary and secondary peaks were observed at 1650 and 1357 cm^{-1} (both of them correspond to the C–C stretching vibration of the benzene ring), with several other weak bands. In this case, Ag NPs show the highest SERS intensity as compared with other NP probes. In the case of TMCA, the SERS spectra showed an intense band at 1340 cm^{-1}, along with weak bands occurring at 1080, 1257, and 1417 cm^{-1}. In our study, we used an Ar^+ ion laser (wavelength 514.5 nm) to obtain the Raman spectra. Thus, the SPR peak of Au NPs (525 nm) is much closer to the excitation wavelength than are those of Ag (403 nm) and Ag@Au (423 nm) NPs. Despite significant overlap between the SPR band and the excitation wavelength, Au NPs yielded the lowest SERS intensities in both cases

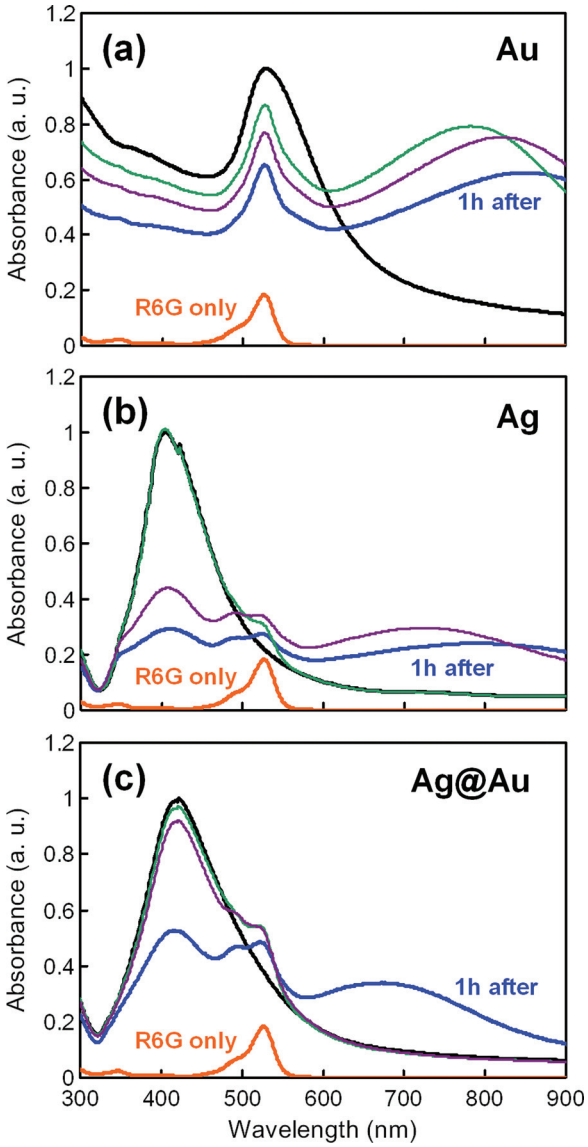

FIG. 5. (Color online) From top to bottom, UV-Vis absorption spectra of as-synthesized, just after adding R6G, after subsequent addition of NaCl, and R6G assembled NPs after 1 hour for (a) Au, (b) Ag and (c) Ag@Au NPs. The bottom curve represents the UV-Vis spectrum of an aqueous solution of only R6G.

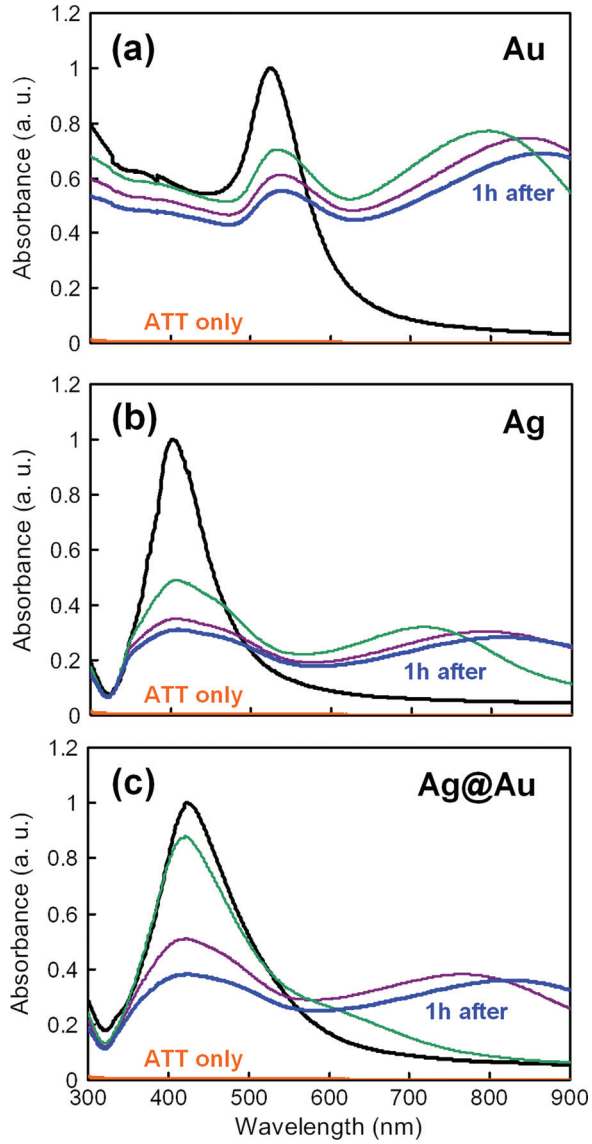

FIG. 6. (Color online) From top to bottom, UV-Vis absorption spectra of as-synthesized, just after adding ATT, after 15 min, and ATT assembled NPs after 1 hour for (a) Au, (b) Ag and (c) Ag@Au NPs. The bottom curve shows the UV-Vis spectrum of an aqueous solution of only ATT.

(vdWA and TMCA), indicating that Au NPs are less efficient probes than are Ag and Ag@Au NPs, as expected. On the other hand, the SPR peak wavelengths of Ag and Ag@Au NPs are almost identical, and thus we can compare both types of NPs consistently. It is noteworthy that the SPR peak wavelength of Ag@Au NPs can be readily varied and tuned by changing the Au shell thickness. In this way, the SPR band can be matched to the fixed frequencies of more economical and readily available laser sources in order to achieve the highest possible enhancement factors.

To quantitatively compare the SERS activities of each NP assembly, the enhancement factors were estimated according to the following procedure.[45] To calculate the enhancement factors, some assumptions were made: (i) NPs form a randomly close-packed structure composed of spheres with a density limit of 63.4%,[46] (ii) the laser spot diameter is 1 μm and the depth (thickness of the deposited assembly) is 1 μm, and (iii) the surfaces of NPs are completely covered by the R6G or ATT molecules (the projected areas of R6G and ATT molecules are 2.01 nm^2 and 0.283 nm^2, respectively). Then, we calculated the number of molecules analyzed under the laser beam for the Ag and Ag@Au NP assemblies. By calculating the ratio between the Raman intensity of only a single Raman reporter molecule from the NP enhanced spectra and the nonenhanced neat spectrum, we estimated the enhancement factor for the cases involving Ag and Ag@Au NPs. In the case of vdWA, the enhancement factor for Ag NPs (4957) was approximately four times higher than that of Ag@Au NPs (1157). This result suggests that the Au shell attenuates the Raman enhancement effect of the Ag core. On the other hand, in the case of TMCA, Ag and Ag@Au NPs showed nearly equal enhancement factors. The calculated enhancement factors for Ag and Ag@Au NPs are 23.5 and 19.5, respectively. These results can be explained in terms of the different chemical natures of the

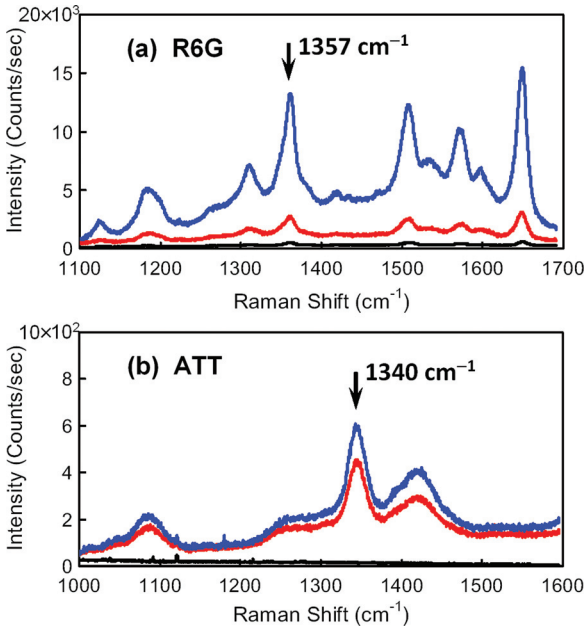

FIG. 7. (Color online) Raman spectra of NP assemblies created by using (a) R6G and (b) ATT. From top to bottom, the spectra of Ag, Ag@Au and Au NP assemblies. Peaks indicated by arrows are used for calculation of enhancement factor.

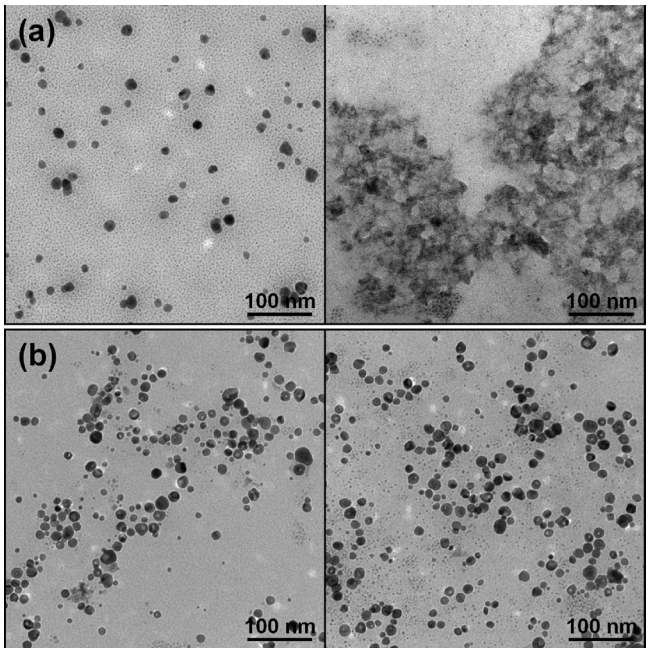

FIG. 8. TEM images of (a) Ag and (b) Ag@Au NPs before (left) and 1 h after (right) adding NaCl.

two reporter molecules and of the mechanism of interaction with the NP surfaces. In the vdWA system, we used R6G dye molecule for the assembly of NPs utilizing the screening of electrostatic repulsion. All NPs are capped by negatively charged citrate ions, and thus the interaction strength between the NP surfaces and the R6G is the same regardless of the composition of the NPs. In the TMCA system, however, we used the thiol-containing ATT molecule, in which NP assembly occurs via metal–sulfur bonding on the surface of particles followed by the electrostatic interaction between the negatively charged citrate ions on the NP surfaces and the positively charged amine groups in the ATT molecules. Because the Au–S interaction is stronger than the Ag–S interaction, the number of ATT molecules adsorbed on the surface of a single Ag@Au NP is expected to be larger than that on a Ag NP. When calculating the enhancement factor, we assumed that the surfaces of the NPs are completely covered by ATT molecules regardless of the type of NP. In reality, however, the number of ATT molecules in the Ag@Au NP assembly would be much larger than that in the Ag NP assembly. That is, Ag NPs essentially have the highest Raman enhancement factor, and Ag@Au NPs have a lower enhancement factor than Ag NPs, likely due to the attenuation effect of the Au shell. Nevertheless, Ag@Au NPs exhibit nearly the same SERS intensity as Ag NPs when the linker molecule contains a thiol group. The most common means of the conjugation of biorelevant molecules onto metal NP surfaces is the utilization of metal–sulfur bonding, which is one reason why Ag@Au NP probes are competitive with Ag NP probes in terms of sensitivity.

D. Assessment of the stability of NPs

One of the main advantages of Ag@Au NPs is their enhanced chemical stability as compared to Ag NPs. Because many kinds of biosensing applications require ambient biological levels of salt during the detection procedure, the stability of the NP probes in the presence of salt should be considered. Therefore, the chemical stability of Ag and Ag@Au NPs in the presence of NaCl was studied. We added 50 μl of NaCl solution (4.8 mM) to 1 ml of NP dispersion. After 1 h, TEM images were taken immediately after preparing the TEM sample. Figure 8 shows TEM images of Ag and Ag@Au NPs taken before and 1 h after adding NaCl. It can be clearly observed that the Ag NPs are almost completely destroyed within 1 h after adding NaCl, while the Ag@Au NPs are mostly intact. These results qualitatively indicate that Ag@Au NPs are superior to Ag NPs as biosensing probes in terms of their interaction with the biological molecule (strong Au–S bonding) and their stability, which makes Ag@Au NP probes superior to monometallic Ag probes in the detection of a wide range of sulfur containing biomolecules.

IV. CONCLUSION

In conclusion, we investigated the SERS activity of Au, Ag, and Ag@Au NPs using two different kinds of Raman active linker molecules. Both R6G and thiol-containing ATT were studied in terms of their activity as Raman probes. It was found that the Ag@Au NPs always have a much higher SERS activity than do Au NPs, and have almost the same activity as Ag NPs when the Raman active linker molecules are adsorbed on the surfaces of NPs via metal–sulfur bonding. In addition, Ag@Au NPs are found to be robust in the presence of salt, whereas Ag NPs are unstable. Based on the results, Ag@Au NPs can be regarded as the most suitable probe for the SERS detection of biomolecules for two reasons. First, metal–sulfur bonding is typically used for the conjugation of biomolecules onto metal NP surfaces.

Second, biosensing protocols frequently require the addition of salt during the detection procedure.

ACKNOWLEDGMENTS

We thank Dr. M. Koyano for his assistance with Raman measurement and K. Higashimine for assistance in the use of TEM and STEM instrumentation.

[1]B. Wiley, Y. Sun, and Y. Xia, Acc. Chem. Res. **40**, 1067 (2007).
[2]L. Lu, A. Kobayashi, K. Tawa, and Y. Ozaki, Chem. Mater. **18**, 4894 (2006).
[3]Y.-S. Shon and E. Cutler, Langmuir **20**, 6626 (2004).
[4]Z. S. Pillai and P. V. Kamat, J. Phys. Chem. B **108**, 945 (2004).
[5]Y.-W. Cao, R. Jin, and C. A. Mirkin, J. Am. Chem. Soc. **123**, 7961 (2001).
[6]Y. Cui, B. Ren, J.-L. Yao, R.-A. Gu, and Z.-Q. Tian, J. Phys. Chem. B **110**, 4002 (2006).
[7]D. Mott, T. B. T. Nguyen, Y. Aoki, and S. Maenosono, Phil. Trans. R. Soc. A **368**, 4275 (2010).
[8]M. J. Hostetler, S. J. Green, J. J. Stokes, and R. W. Murray, J. Am. Chem. Soc. **118**, 4212 (1996); M. J. Hostetler, A. C. Templeton, and R. W. Murray, Langmuir **15**, 3782 (1999); A. C. Templeton, M. J. Hostetler, C. T. Kraft, and R. W. Murray, J. Am. Chem. Soc. **120**, 1906 (1998); A. C. Templeton, M. J. Hostetler, E. K. Warmoth, S. Chen, C. M. Hartshorn, V. M. Krishnamurthy, M. D. E. Forbes, and R. W. Murray, J. Am Chem. Soc. **120**, 4845 (1998).
[9]M. D. Musick, D. J. Pena, S. L. Botsko, T. M. McEvoy, J. N. Richardson, and M. J. Natan, Langmuir **15**, 844 (1999); F. P. Zamborini, J. F. Hicks, and R. W. Murray, J. Am. Chem. Soc. **122**, 4514 (2000); A. C. Templeton, F. P. Zamborini, W. P. Wuelfing, and R. W. Murray, Langmuir **16**, 6682 (2000).
[10]C. A. Mirkin, R. L. Letsinger, R. C. Mucic, and J. J. Storhoff, Nature **382**, 607 (1996); R. Elghanian, J. J. Storhoff, R. C. Mucic, R. L. Letsinger, and C. A. Mirkin, Science **277**, 1078 (1997); T. A. Taton, R. C. Mucic, C. A. Mirkin, and R. L. Letsinger, J. Am. Chem. Soc. **122**, 6305 (2000).
[11]A. K. Boal, F. Ilhan, J. E. DeRouchey, T. Thurn-Albrecht, T. P. Russell, and V. M. Rotello, Nature **404**, 746 (2000); A. K. Boal and V. M. Rotello, J. Am. Chem. Soc. **124**, 5019 (2002); B. L. Frankamp, A. K. Boal, and V. M. Rotello, *ibid.* **124**, 15146 (2002); S. Srivastava, B. L. Frankamp, and V. M. Rotello, Chem. Mater. **17**, 487 (2005).
[12]N. N. Kariuki, L. Han, N. K. Ly, M. J. Patterson, M. M. Maye, G. Liu, and C. J. Zhong, Langmuir **18**, 8255 (2002).
[13]F. L. Leibowitz, W. X. Zheng, M. M. Maye, and C. J. Zhong, Anal. Chem. **71**, 5076 (1999); W. X. Zheng, M. M. Maye, F. L. Leibowitz, and C. J. Zhong, *ibid.* **72**, 2190 (2000); L. Han, J. Luo, N. N. Kariuki, M. M. Maye, V. W. Jones, and C. J. Zhong, Chem. Mater. **15**, 29 (2003).
[14]M. M. Maye, I.-I. S. Lim, J. Luo, Z. Rab, D. Rabinovich, T. Liu, and C. J. Zhong, J. Am. Chem. Soc. **127**, 1519 (2005); I.-I. S. Lim, M. M. Maye, J. Luo, and C. J. Zhong, J. Phys. Chem. B **109**, 2578 (2005).
[15]L. Han, D. R. Daniel, M. M. Maye, and C. J. Zhong, Anal. Chem. **73**, 4441 (2001).
[16]F. P. Zamborini, M. C. Leopold, J. F. Hicks, P. J. Kulesza, M. A. Malik, and R. W. Murray, J. Am. Chem. Soc. **124**, 8958 (2002); M. C. Leopold, R. L. Donkers, D. Georganopoulou, M. Fisher, F. P. Zamborini, and R. W. Murray, Faraday Discuss. **125**, 63 (2004).
[17]L. B. Israel, N. N. Kariuki, L. Han, M. M. Maye, J. Luo, and C. J. Zhong, J. Electroanal. Chem. **517**, 69 (2001).
[18]S. Chen, Langmuir **17**, 6664 (2001); J. Am. Chem. Soc. **122**, 7420 (2000); S. Chen and Y. Yang, *ibid.* **124**, 5280 (2002); J. F. Hicks, F. P. Zamborini, A. J. Osisek, and R. W. Murray, *ibid.* **123**, 7048 (2001).
[19]W. X. Zheng, M. M. Maye, F. L. Leibowitz, and C. J. Zhong, Analyst **125**, 17 (2000).
[20]T. Huang and R. W. Murray, Langmuir **18**, 7077 (2002).
[21]S. K. Ghosh, A. Pal, S. Kundu, S. Nath, and T. Pal, Chem. Phys. Lett. **395**, 366 (2004).
[22]H. Li and L. J. Rothberg, J. Am. Chem. Soc. **126**, 10958 (2004); Anal. Chem. **76**, 5414 (2004).
[23]S. R. Nicewarner-Pena, R. G. Freeman, B. D. Reiss, L. He, D. J. Pena, I. D. Walton, R. Cromer, C. D. Keating, and M. J. Natan, Science **294**, 137 (2001); S. R. Nicewarner-Pena, A. J. Carado, K. E. Shale, and C. D. Keating, J. Phys. Chem. B **107**, 7360 (2003).
[24]D. J. Maxwell, J. R. Taylor, and S. Nie, J. Am. Chem. Soc. **124**, 9606 (2002).
[25]W. Lian, S. A. Litherland, H. Badrane, W. Tan, D. Wu, H. V. Baker, P. A. Gulig, D. V. Lim, and S. Jin, Anal. Biochem. **334**, 135 (2004).
[26]M. D. Malinsky, K. L. Kelly, G. C. Schatz, and R. P. Van Duyne, J. Am. Chem. Soc. **123**, 1471 (2001).
[27]A. J. Haes and R. P. Van Duyne, J. Am. Chem. Soc. **124**, 10596 (2002).
[28]J. C. Riboh, A. J. Haes, A. D. McFarland, C. R. Yonzon, and R. P. Van Duyne, J. Phys. Chem. B **107**, 1772 (2003).
[29]A. D. McFarland and R. P. Van Duyne, Nano Lett. **3**, 1057 (2003).
[30]T. Endo, S. Yamamura, N. Nagatani, Y. Morita, Y. Takamura, and E. Tamiya, Sci. Technol. Adv. Mater. **6**, 491 (2005).
[31]S. Nie and S. R. Emory, Science **275**, 1102 (1997).
[32]K. Kneipp, Y. Wang, H. Kneipp, L. T. Perelman, I. Itzkan, R. R. Dasari, and M. S. Feld, Phys. Rev. Lett. **78**, 1667 (1997).
[33]A. Campion and P. Kambhampati, Chem. Soc. Rev. **27**, 241 (1998).
[34]M. Moskovits, J. Raman Spectrosc. **36**, 485 (2005).
[35]G. A. Baker and D. S. Moore, Anal. Bioanal. Chem. **382**, 1751 (2005).
[36]T. Vo-Dinh, F. Yan, and M. B. Wabuyele, J. Raman Spectrosc. **36**, 640 (2005).
[37]J. Kneipp, H. Kneipp, W. L. Rice, and K. Kneipp, Anal. Chem. **77**, 2381 (2005).
[38]R. Stosch, A. Henrion, D. Schiel, and B. Guttler, Anal. Chem. **77**, 7386 (2005).
[39]T. B. T. Nguyen, R. Yokogawa, Y. Yoshimura, K. Fujimoto, M. Koyano, and S. Maenosono, Analyst **135**, 595 (2010).
[40]Y. C. Cao, R. Jin, J. M. Nam, C. S. Thaxton, and C. A. Mirkin, J. Am. Chem. Soc. **125**, 14676 (2003).
[41]X. Su, J. Zhang, L. Sun, T. W. Koo, S. Chan, N. Sundararajan, M. Yamakawa, and A. A. Berlin, Nano Lett. **5**, 49 (2005).
[42]M. Culha, D. Stokes, L. R. Allain, and T. Vo-Dinh, Anal. Chem. **75**, 6196 (2003).
[43]A. Pyatenko, M. Yamaguchi, and M. Suzuki, J. Phys. Chem. B **109**, 21608 (2005).
[44]I.-I. S. Lim, F. Goroleski, D. Mott, N. Kariuki, W. Ip, J. Luo, and C. J. Zhong, J. Phys. Chem. B **110**, 6673 (2006).
[45]See supplementary material at E-JAPIAU-109-020108 for a full description of this procedure, http://dx.doi.org/10.1063/1.3579445.
[46]C. Song, P. Wang, and H. A. Makse, Nature **453**, 629 (2008).